ELSEVIER

Theoretical description of dry laser cleaning

N. Arnold[*]

Angewandte Physik, J. Kepler University, Altenbergerstraße 69, A-4040 Linz, Austria

Abstract

Dry laser cleaning (DLC) is considered as an escape from an adhesion potential under the forces induced by thermal expansion. Important temporal and spatial scales are: period of small oscillations τ_0, and equilibrium deformation h_0.

Possible cleaning regimes are discussed. With laser pulse duration $\tau < \tau_0$ (large particles) removal is due to elastic energy. With $\tau > \tau_0$ (small particles) cleaning proceeds in the inefficient inertial force regime. If the fronts of the laser pulse are steep enough, $t_f \ll \tau_0$, cleaning occurs when kinetic energy of the particle exceeds that of adhesion.

Utilization of resonance effects by modulation of laser pulse or employing the train of pulses and influence of damping on these regimes are discussed. Effects of the near field focusing by dielectric spheres and decrease in cleaning threshold due to three-dimensional (3D) effects are analyzed and compared with the experimental results for SiO_2 particles on Si surface.
© 2002 Elsevier Science B.V. All rights reserved.

PACS: 42.62.Cf; 81.65.Cf; 68.35.Np; 81.65.-b; 85.40.-e; 81.07.Wx

Keywords: Laser cleaning; Modeling; Threshold; Oscillations; Damping; Focusing

1. Introduction

The physical principles of laser cleaning are outlined in [1]. In studies of dry cleaning (DLC) one usually compares cleaning and adhesion forces [2–4]. Recently it has been realized, that ns DLC requires consideration of dynamic effects [5–7]. Utilization of resonance effects (resonant laser cleaning (RLC)) was suggested [8,9]. In [10], the influence of material parameters and temporal shape of the laser pulses on DLC efficiency was studied theoretically. In the present paper, we give an overview of previous results. Then we discuss the influence of damping on RLC and the possibilities of experimental verification of particle oscillations using several pulses with delay.

Finally, we discuss local intensity enhancement [6,11–13] and resulting three-dimensional (3D) thermal expansion near transparent particle [6].

2. Theoretical framework

Laser cleaning can be formulated as an escape from the potential under the action of a time-dependent force [8,9]. Particle with the radius r and a plane approach by a distance h (see Fig. 1). Approximate potential and force can be written as

$$U = -2\pi r h\varphi + \tfrac{2}{5}\bar{Y}r^{1/2}h^{5/2},$$
$$F = 2\pi r\varphi - \bar{Y}r^{1/2}h^{3/2} \tag{1}$$

Here φ is the work of adhesion (over the contact area $2\pi rh$) and $1/\bar{Y} = 3/4((1 - \sigma^2)/Y + (1 - \sigma_p^2)/Y_p)$ characterizes elastic properties of the substrate and

[*] Tel.: +43-732-24689245; fax: +43-732-24689242.
E-mail address: nikita.arnold@iku.at (N. Arnold).
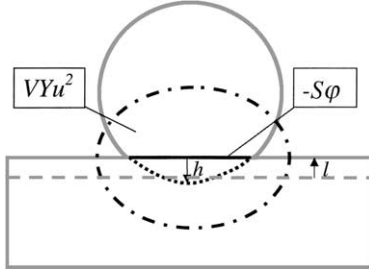
Fig. 1. Simplified schematic of the particle–substrate deformation characterized by h. Solid lines: boundaries of substrate and particles. Dashed line: initial position of the substrate displaced by l. Dotted curve: imaginary non-deformed particle. Dash-dotted oval indicates localization of elastic energy. Surface energy is gained over the contact area S.

the particle (index "p"). Y is Young modulus and σ the Poisson ratio. Equilibrium values of h_0 and U_0 are

$$h_0 = \left(\frac{2\pi\varphi}{\bar{Y}}\right)^{2/3} r^{1/3},$$
$$U_0 = -\frac{3}{5}(2\pi\varphi)^{5/3}\bar{Y}^{-2/3}r^{4/3} \qquad (2)$$

Detachment occurs with $h = 0$ and requires pull-out force $F_0 = 2\pi r\varphi$. Parabolic approximation to the potential (1) yields frequency ω_0 and period $\tau_0 = 2\pi/\omega_0$ of small oscillations

$$\tau_0 = \frac{5^{1/2}(2\pi)^{4/3}}{3}\left(\frac{r^7\rho_p^3}{\varphi\bar{Y}^2}\right)^{1/6} \qquad (3)$$

This is about 10 ns for $r = 1\ \mu$m and typical material parameters.

Let l be the surface displacement in the *laboratory* frame. Then Newton equation with the force (1) in the reference frame fixed with the substrate reads (dot stands for time derivative and m is the particle mass)

$$\ddot{h} + \gamma\dot{h} + \frac{1}{m}\frac{\partial U}{\partial h} = \ddot{l} \qquad (4)$$

The value of damping coefficient γ is discussed in [8,9]. For quasi-static unilateral expansion of the substrate surface displacement l and velocity are given by [9]

$$l(t) = \frac{1+\sigma}{1-\sigma}\frac{\beta\phi_a(t)}{3c\rho}, \quad \dot{l} = \frac{1+\sigma}{1-\sigma}\frac{\beta I_a(t)}{3c\rho} \qquad (5)$$

Here ϕ_a and I_a are absorbed fluence and intensity, c and ρ are specific heat and density of the substrate and

β volumetric coefficient of thermal expansion. Laser pulse is approximated by

$$I(t) = I_0\frac{t}{\tau}\exp\left(-\frac{t}{\tau}\right) \qquad (6)$$

With this definition $\phi = I_0\tau$, maximum intensity $I_{\max} = I(\tau) = I_0 e^{-1}$ and the full-width at half-maximum pulse duration $\tau_{\text{FWHM}} \approx 2.45\tau$.

3. One-dimensional (1D) consideration

3.1. Single pulse threshold, three regimes

The model reveals three possible cleaning regimes. With $\tau \ll \tau_0$, which corresponds to large particles or short pulses, particle barely moves during the pulse. Thermal expansion compresses both the particle and the substrate, and at the end of the pulse they possess elastic energy. If it is larger than the total adhesion energy and if damping is small, this results in "elastic energy" removal. Because adhesion potential is almost symmetric near the equilibrium, the particle is removed in the first backward swing of oscillations after the pulse, if compression was larger than the equilibrium deformation.

With $\tau \gg \tau_0$, which corresponds to small particles or long pulses, the particle moves with the substrate and detaches when thermal expansion decelerates at the trailing front of the pulse. Here cleaning (inertia) force should overcome adhesion force. Similar conditions hold for strong damping. This is "force" regime, which favors shorter pulses.

If the thermal expansion stops sharply, the force of inertia becomes very large. This may happen if the laser pulse has steep fronts, $t_f \ll \tau_0$. Cleaning occurs if kinetic energy acquired by the particle exceeds that of adhesion.

For parameters of adhesion potential from Section 2 and 1D expansion of the substrate given by Eq. (5) the results for cleaning fluence ϕ_{cl} can be summarized as follows:

$$\begin{array}{ll} \tau \ll \tau_0 & l > h_0 \Rightarrow \phi_{cl} \propto r^{1/3} \\ \tau \gg \tau_0 & -m\ddot{l}_{\max} > F_0 \Rightarrow \phi_{cl} \propto \tau^2/r^2 \qquad (7) \\ \tau \gg \tau_0,\ t_f \ll \tau_0 & m\dot{l}_f^2/2 > |U_0| \Rightarrow \phi_{cl} \propto \tau/r^{5/6} \end{array}$$

Particle expansion can be included by replacing $l \to l + \Delta r$ [8,9]. Detailed studies of these regimes,
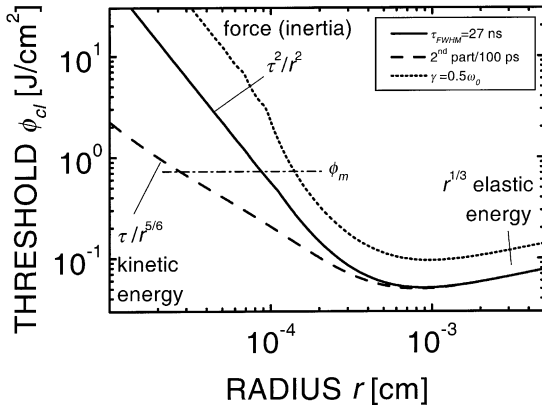
Fig. 2. Three regimes of DLC. In all pictures parameters are the same as in Table 1 in [10]. Laser pulse is given by the Eq. (6). Solid curve: $\tau_{FWHM} = 27$ ns. Dashed curve: second part of this pulse ($t > \tau$) with the leading front rise time $\tau_f = 100$ ps. Dotted curve: damping coefficient $\gamma = 0.5\omega_0$. Dash-dotted line: large-area melting threshold.

numerical coefficients and dependences on the pulse and material parameters are presented in [10]. Fig. 2 shows calculated thresholds for a smooth pulse and for a pulse with steep front. Dotted curve demonstrates the influence of damping. Strong damping increases the threshold, but does not change the functional dependence on particle radius.

3.2. Oscillations, damping

The existence of internal oscillations in the particle-on-surface system suggests the usage of resonance effects. Resonant laser cleaning (RLC) was studied theoretically in [10]. Crucial question is the value of damping coefficient γ. Physical mechanisms of damping are discussed in [8,9]. The strongest damping may be due to the emission of sound waves from the oscillating region. Fig. 3 shows the calculated threshold for a pulse modulated with 10 oscillations. Even with appreciable damping, $\gamma = 0.2\omega_0$, resonant effects can be seen. If the oscillations become overdamped (dotted curve), resonant dip in cleaning fluence disappears.

3.3. Train of pulses

Before developing experimental setup for RLC, one has to verify or disprove experimentally the existence
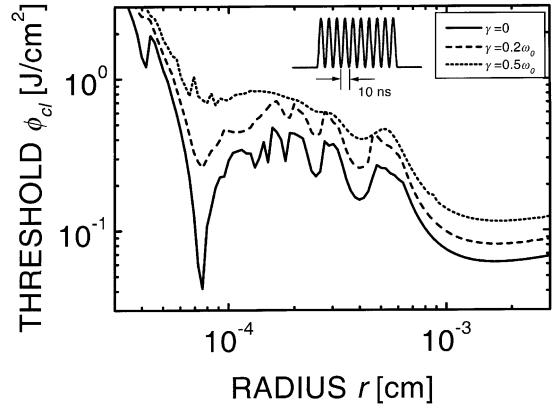
Fig. 3. Resonance effects. Pulse with the total duration $\tau = 100$ ns is sinusoidaly modulated at 100 MHz (10 oscillations, see inset). The values of damping coefficient are given in the legend.

of particle oscillations. One possibility is to excite them by a short (sub-ns) "pump" pulse and to apply a second "probe" pulse with delay τ_d. If the second pulse arrives in the right moment, it improves cleaning. The expected result is shown in Fig. 4. The horizontal parts of the $\phi_{cl}(\tau_d)$ dependence correspond to the cleaning by the first pulse alone. The minima correspond to $\tau_d \approx \tau_0$, when the pulses arrive "in phase" and their contributions combine. The threshold
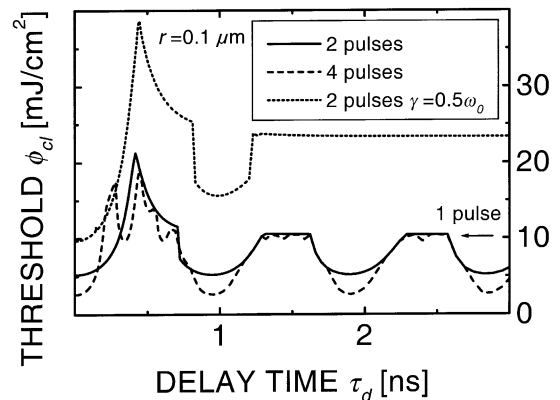
Fig. 4. Cleaning by several pulses with delay time τ_d. ϕ_{cl} refers to a fluence of a single pulse. Parameters used in the calculations are: Gaussian temporal profile of the pulse with $\tau_{FWHM} = 300$ ps, absorptivity $A = 0.7$, (this corresponds to a Ti:Sa laser with $\lambda = 800$ nm). $r = 0.1$ μm, i.e. $\tau_0 = 1.05$ ns. Solid curve: two pulses without damping. Dashed curve: four pulses. Dotted curve: two pulses with damping $\gamma = 0.5\omega_0$.

decrease in these minima is proportional to the number of pulses. Even with strong damping (dotted curve) the first decrease in threshold with delay time can be clearly seen. The maximum corresponds to the $\tau_d \approx \tau_{FWHM}$. Here, the pulses merge in one longer, less effective pulse with complex shape.

4. Influence of local intensity and 3D expansion on cleaning

Up to now, we considered 1D substrate heating and expansion unaffected by the presence of the particle. It has been realized lately [6,11–13], that the particle may significantly change local intensity distribution. This will lead to local 3D heating and thermal expansion. In the first approximation, it should be added to 1D expansion. The latter remains unchanged, as particles cover only small fraction of substrate surface. Elastic disturbance propagates with the velocity of sound v_0 and thermoelastic problem near the particle can be considered quasi-statically for $t \gg r/v_0 \sim 0.1$ ns.

To study cleaning threshold over the large range of parameters, several simplifications are employed. We approximate local particle-induced intensity by a Gaussian beam with the effective spot size w and intensity in the center $I_m \equiv M I_0$. Here I_0 is the intensity of the incident light and M intensity enhancement. Note, that heat conduction smears out fine structure of intensity distribution. We assume that the contact area between the particle and the substrate is small and for I in the cleaning Eq. (4) we use *epicentral* 3D expansion.

The 3D quasi-static expansion with the stress relaxation at infinity is discussed in Appendix A. Expression (A.8) was used in the calculations. Here central intensity $I_a(t)$ absorbed at the surface is assumed. For the pulse (6) l can be expressed in terms of exponential integrals. To proceed further we have to know how the spot size $w(r)$ and intensity enhancement $M(r)$ change with particle radius. To obtain compact estimations, we consider in Appendix B two simplified cases: geometrical optics and dipole approximation. Formulas (B.5) for $w(r)$ and (B.4) for $M(r)$ were used in calculations. Though the formulas were derived for transparent (silica) spheres with refractive index $1.1 < n < 1.9$, the conclusions hold also for non-spherical particles, as caustics and dipole-plane wave interference are modified, but still exist in the general case.
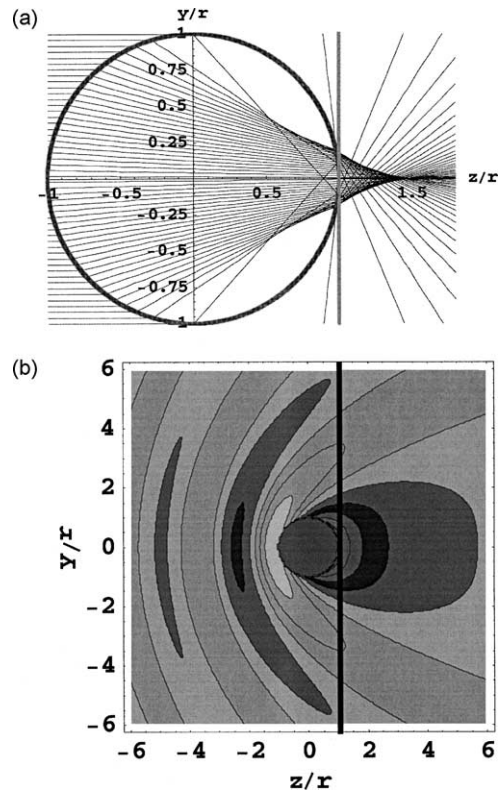
Fig. 5. Influence of transparent sphere on local intensity distribution. (a) Large sphere $r \gg \lambda$. Majority of rays hitting the substrate are confined within the caustic cone. (b) Interference between the plane incident wave propagating into positive z-direction and dipole radiation from the small sphere $r = 0.2\lambda \ll \lambda$. Refractive index $n = 1.5$. Incident wave is polarized along x-direction.

Two limiting cases discussed in Appendix B are shown in Fig. 5. Substrate is at $z = r$ and is not included in calculations. We are interested in the intensity on the substrate immediately behind the sphere, not in the focal intensity. This makes estimations easier, especially for large spheres, as focal region is much stronger affected by the spheres' imperfections, while caustic or dipole field are only distorted.

Fig. 6 illustrates the relative importance of 1D and 3D effects for the $r = 1$ μm particle, when the enhancement is strong, $I_m/I_0 = 24.4$. As a result 3D temperature is significantly higher than 1D (with *equal* intensities 3D temperature is always lower). The 1D and the 3D thermal expansions are comparable, but velocity and acceleration are larger for 3D contribution due to faster, more transient 3D expansion.
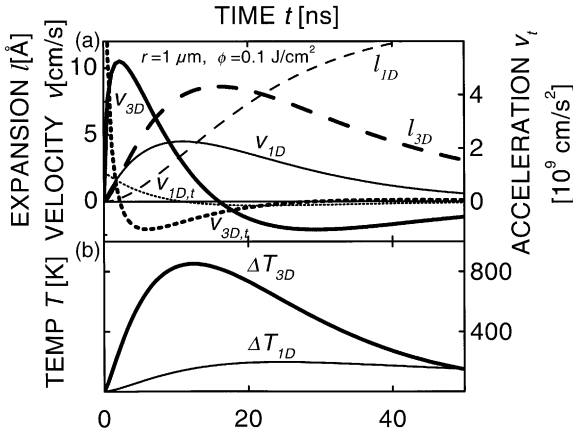
Fig. 6. Contribution of 1D and 3D effects. Parameters used in the calculation: particle radius $r = 1$ μm, wavelength $\lambda = 0.248$ μm. Substrate thermal diffusivity $D = 0.5$ cm^2/s, absorptivity $A = 0.5$, fluence $\phi = 0.1$ J/cm^2. (a) Dashed curves: surface displacement l. Solid curves: surface velocity v. Dotted curves: acceleration v_t. Thin curves refer to 1D, thick to 3D contributions. Subplot (b) shows temperature rise.

Fig. 7 summarizes the influence of 3D effects on DLC. With small sub-wavelength particles (of arbitrary shape) $r < \lambda/2$, small dipole moment leads to a sharp (quadratic, see (B.3)) decrease in excess 3D intensity. Correspondingly, all 3D contributions become small, though acceleration decreases not as fast as temperature, due to different functional dependence of the acceleration (A.7) in this region (Fig. 7b). Cleaning of the sub-wavelength particles is most important for the needs of technology. Field enhancement effects become increasingly unimportant in this region. Nevertheless, due to high overall intensities in this region one can expect melting there, both in 1D and in 3D model.

When particle diameter exceeds several λ, intensity enhancement M and w/r ratio approach their geometrical values, while effective spot size w grows proportionally to r. Temperature and expansion velocity increases weaker than intensity. This is related to lateral heat conduction and to 3D relaxation of stresses for smaller spots. With very large particles $w(r) \geq 2(Dt)^{1/2}$; thermal expansion becomes 1D, and is described by (15). Here the ratio of all 3D/1D contributions is determined by the geometrical optical intensity enhancement (B.2).

Though focusing is stronger for larger particles, the temperature *values* near threshold decrease in this region, due to decrease in threshold fluence.
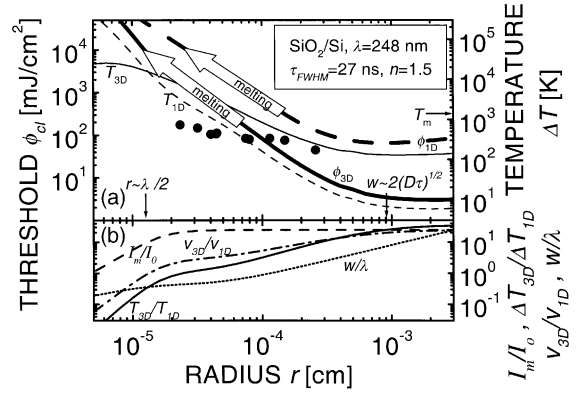
Fig. 7. Calculated influence of local 3D effects on cleaning threshold. Diffusivity $D = 0.32$ cm^2/s, absorptivity $A = 0.39$, which corresponds to a Si at $\lambda = 0.248$ μm. (a) Cleaning threshold. Dashed curve: only 1D heating and expansion. Solid curve: 1D and 3D expansions are added. Thin lines: corresponding temperature rises. Circles: experimental points from [8]. Large arrows indicate theoretical onset of melting in both models. Subplot (b) shows contributions of different factors. Solid curve: ratio of expansion velocities; dashed curve: intensity enhancement M, Eq. (B.4); dotted curve: ratio of effective Gaussian spot size to wavelength calculated from Eq. (B.5). Dash-dotted curve: ratio of induced temperature rises.

Experimental results obtained with 248 nm KrF laser radiation [8] (circles) are much more consistent with the 3D model. Still, the slope of $\phi_{cl}(r)$ dependence is different. The discrepancy may be related to onset of local ablation observed in the experiments [11,12,14] and references therein. This is consistent with high estimated temperatures for small particles (Fig. 7a, thin solid line).

The 3D temperature has a maximum at $r \sim 60$ nm. As exact values of 3D/1D velocity and temperature ratios depend on the temporal profile of laser pulse, we give here approximate formulas. They reasonably agree with the numerical results shown in Fig. 7b.

$$\frac{v_{3D}}{v_{1D}} \sim 2(1 - \sigma)M \frac{w^2}{8D\tau} \ln\left(1 + \frac{8D\tau}{w^2}\right) \tag{8}$$

$$\frac{\Delta T_{3D}}{\Delta T_{1D}} \sim M \frac{w}{2\sqrt{D\tau}} \arctan\left(\frac{2\sqrt{D\tau}}{w}\right) \tag{9}$$

5. Conclusions

We considered the DLC as an escape from the adhesion potential under the action of a cleaning force

induced by thermal expansion. Apart from pull-out force F_0, the parameters of the adhesion potential important for DLC are the period of oscillations τ_0 and equilibrium deformation h_0. With laser pulse duration $\tau < \tau_0$ (big particles) cleaning takes place in the "elastic energy" regime. This requires that overall thermal expansion $l > h_0$ resulting in $\phi_{cl} \propto r^{1/3}$. With $\tau > \tau_0$ (small particles) cleaning occurs in the "inertial force" regime, which requires decelerations $-m\ddot{l}_{max} > F_0$, leading to $\phi_{cl} \propto \tau^2/r^2$. With $\tau > \tau_0$, but steep edges of the pulse $t_f \ll \tau_0$, cleaning requires that particle kinetic energy exceeds that of adhesion $m\dot{l}_f^2/2 > |U_0|$. This leads to $\phi_{cl} \propto \tau/r^{5/6}$. Utilization of resonance effects by modulation of laser pulse or using the train of pulses is discussed. Resonant effects are present even with significant damping. Local intensity enhancement and 3D thermal expansion near the particle decrease calculated DLC threshold by about an order of magnitude, but weakly change the functional dependences. The approach and conclusions remain valid for non-spherical particles.

Acknowledgements

Appendix A. Epicentral surface displacement in quasi-static 3D thermal expansion

In [9], we derived the expression for the surface displacement l due to thermal expansion when heating should be considered as 3D with time-dependent temperature distribution

$$\tilde{l} = \beta_3 \int_0^\infty e^{-kz} \tilde{T}(z)\,dz, \quad \beta_3 \equiv \tfrac{2}{3}\beta(1+\sigma) \qquad (A.1)$$

Here, tilde denotes Fourier components of functions with wavevector $\boldsymbol{k}$ (length k) after transformation in x–y plane. It is desirable to relate this expression to the temporal profile of laser pulse to avoid solution of the heat equation. We use heat equation with constant coefficients, volume absorption and no heat losses [1]. Temperature is referred to the ambient temperature. After Fourier transform it reads together with boundary conditions.

$$\dot{\tilde{T}} = (\tilde{T}_{zz} - k^2\tilde{T}) - \frac{\tilde{I}_z}{c\rho}$$
$$\tilde{T}_z|_{z=0} = 0, \quad \tilde{T}|_{z\to\infty} \to 0 \qquad (A.2)$$

Here D is the thermal diffusivity and subscript z stands for differentiation. We differentiate (A.1) with respect to time and substitute $\dot{\tilde{T}}$ from (A.2). Upon integration over z one obtains

$$\dot{\tilde{l}} = \beta_3 \left[-Dk\tilde{T}(0) - \int_0^\infty e^{-kz}\left(\frac{\tilde{I}_z}{c\rho}\right)dz \right]$$
$$= \frac{\beta_3}{c\rho}\left[\tilde{I}(0) - k\int_0^\infty e^{-kz}\tilde{I}\,dz - Kk\tilde{T}(0) \right] \qquad (A.3)$$

Fourier inversion of the first term yields absorbed intensity, albeit with somewhat different coefficient than in 1D case. For further simplifications we assume Bouguer absorption with absorption coefficient α. Then $\tilde{T}(0)$ can be found from the Eq. (A.2) by substitution $\tilde{T} = \tilde{T}_1 e^{-Dk^2 t}$. This removes the term with k^2 in the RHS and Green's function formulas for the 1D heat equation [1] can be applied. This results in

$$\dot{\tilde{l}} = \frac{\beta_3}{c\rho}\left[\frac{\alpha}{\alpha+k}\tilde{I}(0) - Kk\frac{\alpha}{c\rho}\int_0^t e^{D(\alpha^2-k^2)t_1}\right.$$
$$\left. \text{erfc}(\alpha\sqrt{Dt_1})\tilde{I}(0, t-t_1)\,dt_1 \right] \qquad (A.4)$$

The integration can be carried out for constant intensity, but the inversion of Fourier transform is still problematic. Compact formulas can be obtained for surface absorption $\alpha \to \infty$ and Gaussian beam with the spot size w. Then $e^{D\alpha^2 t_1}\text{erfc}(\alpha\sqrt{Dt_1}) \to 1/\alpha\sqrt{\pi D t_1}$ and inversion can be carried out. For epicentral displacement $r = 0$.

$$\dot{l} = \frac{\beta_3}{c\rho}\left[I_a(t) - \int_0^t \frac{\dot{I}_a(t-t_1)}{\sqrt{1+w^2/4Dt_1}}\,dt_1 \right]$$
$$= \frac{\beta_3}{c\rho}\left[\int_0^t \dot{I}_a(t-t_1)\left(1 - \frac{1}{\sqrt{1+w^2/4Dt_1}}\right)dt_1 \right]$$
$$\qquad (A.5)$$

The first expression required integration by parts. In the last expression, we replaced $I_a(t) \rightarrow \int_0^t I_a(t - t_1)\, dt_1$. One can distinguish two limiting cases. With thermally large spots $D\tau/w^2 \ll 1$, $1/\sqrt{1 + w^2/4Dt_1} \rightarrow 0$ and

$$\dot{l} \approx \frac{2(1 + \sigma)}{3} \frac{\beta I_a(t)}{c\rho} \tag{A.6}$$

This recovers 1D result with 3D stress relaxation discussed in [9]. With small spots, $D\tau/w^2 \gg 1$, the region near $t_1 = 0$ dominates the integral (A.5). With $\dot{I}_a(t - t_1) \approx \dot{I}_a(t)$ the leading term yields

$$\dot{l} \approx \frac{2(1 + \sigma)}{3} \frac{\beta \dot{I}_a(t)}{c\rho} \frac{w^2}{4D} \operatorname{arcsinh}\left(\frac{2\sqrt{Dt}}{w}\right) \tag{A.7}$$

Velocity (and acceleration) *decrease* with thermal diffusivity as transient temperature rise is smaller. In the first expression in (A.5) the integral is manifestly positive and therefore $\dot{l} < \beta_3 I_a(t)/c\rho$. Similar statement almost always holds for the (absolute value of) acceleration.

For practical purposes we approximate the kernel in the last integral (A.5) in a way that is asymptotically correct for both small and large t_1

$$\dot{l} \approx \frac{\beta_3}{c\rho}\left[\int_0^t \frac{\dot{I}_a(t - t_1)}{1 + 8Dt_1/w^2}\, dt_1\right] \tag{A.8}$$

This results in approximation for $D\tau/w^2 \gg 1$ that are slightly better than (A.7) for intermediate τ.

$$\dot{l} \approx \frac{2(1 + \sigma)}{3} \frac{\beta \dot{I}_a(t)}{c\rho} \frac{w^2}{8D} \ln\left(1 + \frac{8Dt}{w^2}\right) \tag{A.9}$$

Appendix B. Sphere focusing approximations

Exact calculations of the field distribution near the particle on the surface use numerical methods [11], analytical Mie solution in free space [6,12] or in the presence of the substrate [13]. To obtain compact estimations we consider two simplified cases.

B.1. Large spheres, $r \gg \lambda$, geometrical optics

Let us estimate the intensity on the substrate using ray tracing and energy conservation. Refracted rays form a caustic (Fig. 5a). Almost all the rays that reach the substrate, lie within the caustic cone. We introduce the

incidence angle θ_i and the refraction angle inside the sphere $\theta_t = \arcsin(\sin\theta_i/n)$. Upon second refraction the ray leaves the sphere at a point with the polar angle with the z-axis $\theta_o = 2\theta_t - \theta_i$, and emerges from the sphere in the direction $\theta_{ou} = 2\theta_t - 2\theta_i < 0$. Maximizing $\theta_o(\theta_i)$ we find that the caustic crosses the sphere at the angle θ_{om}, given by the condition $\sin^2\theta_{om} = (4 - n^2)^3/27n^4$. Corresponding angle of incidence θ_{im}, is given by $\sin^2\theta_{im} = (4 - n^2)/3$. We approximate the spot size on the substrate by caustic on the sphere

$$w_g \approx r\sin\theta_{om} = r\sqrt{\frac{(4 - n^2)^3}{27n^4}} \tag{B.1}$$

Rays that emerge with the angles $\theta_{ou} < -\pi/2$ propagate backwards and do not contribute to the intensity on the substrate. This results in $2\theta_t - 2\theta_i = -\pi/2$, which limits the relevant incoming rays by a condition

$$\sin^2\theta_{i,\pi/2} = \begin{bmatrix} 1, & n < \sqrt{2} \\ \dfrac{n^2}{2n(n - \sqrt{2}) + 2}, & n > \sqrt{2} \end{bmatrix}$$

The incident radiation is homogeneous. We assume that the intensity within the caustic cone is homogenized by the imperfections of the sphere, reflections from the substrate, etc. Thus we neglect any interference and resonance effects. Assuming $r_0 = r\sin\theta_{i,\pi/2}$ for the maximal impact parameter of incoming rays, we obtain for intensity enhancement

$$\frac{I_m}{I_0} \approx \frac{r_0^2}{w_g^2} \approx \frac{r^2\sin^2\theta_{i,\pi/2}}{r^2\sin^2\theta_{om}}$$

$$= \frac{27n^4}{(4 - n^2)^3}\begin{bmatrix} 1, & n < \sqrt{2} \\ \dfrac{n2}{2n(n - \sqrt{2}) + 2}, & n > \sqrt{2} \end{bmatrix} \tag{B.2}$$

We neglect intensity losses on reflection as they are to some degree counterbalanced by multiple reflections within the sphere and from the substrate surface. In some cases, e.g. with n close to 1 or $n > 2$ this approximation is less accurate. One should consider the caustic spot on the substrate and the rays with $\theta_o < 0$ but $\theta_{ou} < -\pi/2$ widen the actual spot. For the sake of simplicity, we do not discuss this here.

B.2. Small spheres, $r \ll \lambda$, dipole approximation

Small spheres can be approximated by dipoles with corresponding polarizability [15]. Using the formulas

(92.1), (92.2) and considering interference with the incident plane wave at the back side of the sphere at $z = r$, we obtain

$$\frac{I_m}{I_0} = \left(1 + \frac{n^2 - 1}{n^2 + 1} k^2 r^2\right)^2 \tag{B.3}$$

The size of the spot is $w_d \approx r$ within the range of applicability of dipole approximation.

B.3. Approximation for all sizes

As we are interested with the excess intensity due to the presence of the particle we introduce excess intensity amplification for geometrical (g) and dipole (d) cases respectively $M_{g,d} \equiv (I_m / I_0) - 1$, To span all sizes, we use the approximation of dipole and geometrical enhancement, which smoothly combines both limiting cases.

$$M \approx \frac{M_d M_g}{M_d + M_g} \tag{B.4}$$

For the spot size we employ

$$w = \frac{w_d + C k^2 r^2 w_g}{1 + C k^2 r^2} \tag{B.5}$$

with

$$C = \frac{n^2 - 1}{n^2 + 1} \sqrt{\frac{(4 - n^2)^3}{27 n^4}}$$

This choice of C ensures that the transition between the limiting cases (which happens with $C k^2 r^2 \sim 1$) occurs when $M_d \sim M_g$.

References

[1] D. Bäuerle, Laser Processing and Chemistry, 3rd ed., Springer, Berlin, 2000.

[2] V. Dobler, R. Oltra, J.P. Boquillon, M. Mosbacher, J. Boneberg, P. Leiderer, Appl. Phys. A 69 (1999) 335.

[3] Y.F. Lu, W.D. Song, B.W. Ang, M.H. Hong, D.S.H. Chan, T.S. Low, Appl. Phys. A 65 (1997) 9.

[4] V.P. Veiko, E.A. Shakhno, S.V. Nikolaev, Proc. SPIE 4088 (2000) 179.

[5] Y.F. Lu, Y.W. Zheng, W.D. Song, Appl. Phys. A 68 (1999) 569.

[6] B.S. Luk'yanchuk, Y.W. Zheng, Y.F. Lu, Proc. SPIE 4423 (2001) 115.

[7] G. Vereecke, E. Röhr, M.M. Heyns, J. Appl. Phys. 85 (1999) 3837.

[8] N. Arnold, G. Schrems, T. Mühlberger, M. Bertsch, M. Mosbacher, P. Leiderer, D. Bäuerle, Proc. SPIE 4426 (2002) 340.

[9] N. Arnold, Dry laser cleaning of particles by nanosecond pulses: theory, in: B. Luk'yanchuk (Ed.), Laser Cleaning, Word Scientific, Singapore, 2002, Chapter 2, pp. 51–96.

[10] N. Arnold, Appl. Surf. Sci. 197–198 (2002) 904.

[11] H.-J. Münzer, M. Mosbacher, M. Bertsch, O. Dubbers, A. Pack, R. Wannemacher, B.-U. Runge, D. Bäuerle, P. Leiderer, Proc. SPIE 4426 (2002) 180.

[12] H.-J. Mtinzer, M. Mosbacher, M. Bertsch, J. Zimmermann, P. Leiderer, J. Boneberg, J. Microsc. 202 (2001) 129.

[13] B.S. Luk'yanchuk, Y.W. Zheng, Y.F. Lu, Proc. SPIE 4065 (2000) 576.

[14] Y.F. Lu, L. Zhang, W.D. Song, Y.W. Zheng, B.S. Luk'yanchuk, JETP Lett. 72 (2000) 457.

[15] L.D. Landau, E.M. Lifshitz, L.P. Pitaevskii, Electrodynamics of Continuous Media, Pergamon Press, New York, 1984.